Control of MEMS-Technology Axial Topology MicroServos

Sergey Edward Lyshevski and Avnish P. S. Chauhan
Department of Electrical and Microelectronic Engineering
Rochester Institute of Technology, Rochester, NY 14623, USA
E-mail: E.Lyshevski@rit.edu and Sergey.Lyshevski@mail.rit.edu

ABSTRACT

Micro-electromechanical systems (MEMS) integrate MEMS-technology sensors, actuators and integrated circuits (ICs). High-performance electromagnetic microscale sensors and actuators with matching ICs are designed and tested. These MEMS-technology actuators are uniquely suit biotechnology, medicine, robotics and other applications where high force and torque are needed. We examine close-loop electromagnetic mini actuators and servos with controlling ICs. Complete MEMS systems with minidrives and servos are designed, optimized, tested and characterized.

Keywords: actuator, integrated circuits, micro electromechanical system, servosystem

1. INTRODUCTION

In many applications, stringent specifications are imposed on performance and capabilities of actuators. In the expanded operating envelopes, a broad spectrum of requirements and specifications can be achieved using MEMS-technology sensors and electromagnetic actuators [1, 2]. Conventional electrostatic actuators do not guarantee the desired force (torque) and energy densities. Therefore, electromagnetic solutions must be applied [2]. Recently, electromagnetic MEMS with permanent magnets were fabricated and widely deployed. In particular, AlNiCo and rare-earth (SmCo and NdFeB) magnets guarantee very high energy densities which is defined by $BH_{\max}$ [1, 2].

For high-performance systems, a concurrent MEMS design, fabrication, optimization and hardware-software co-design have become major challenging themes. The major goal of this paper is to report, apply and demonstrate enabling concepts in design and optimization of advanced technology MEMS. We examined radial and axial topology actuators. An axial-topology solution guarantees significant fabrication, structural and integration advantages. In fact:

1. Electromagnetic system is optimized and guarantees superior force (torque) and energy densities;
2. Electromagnetic and mechanical systems are coupled and integrated enabling *direct-drive* solutions and minimizing complexity;
3. Multi-layer planar windings are straightforwardly deposited;
4. There is no need for ferromagnetic materials;
5. Miniscale permanent magnets (and magnetic arrays) of any size, geometry, magnetization and strength are placed or encapsulated guarantying the overall consistency;
6. Actuator, sensors and ICs are integrated;
7. Simplicity, affordability and high yield are ensured;
8. Operating envelope is expanded; etc

Axial-topology high-torque density actuators with permanent-magnet arrays ensure superior performance. For miniscale hard drives, our actuators ensure high precision, fast (minimal time) repositioning, efficiency, robustness, etc. We design and implement various control laws in order to guarantee *near optimal* performance and capabilities. These control laws are implemented using analog and digital ICs. ICs controllers/drivers vary the voltage, and the measurements on the state variables and output are used.

This paper examines and solves a spectrum of pertinent problems in design and optimization of MEMS, miniactuators and miniservos. Advanced engineering solutions and enabling technologies are examined in various applications.

2. HIGH-PERFORMANCE MINISCALE ACTUATORS AND SERVOS

We examine high-performance actuators. The Poynting vector $\mathcal{P}$, which is a power density vector, represents the power flows per unit area. We have, $\mathcal{P}=\mathbf{E}\times\mathbf{H}$. Furthermore,

$$\oint_s (\mathbf{E}\times\mathbf{H})\cdot d\mathbf{s} = \frac{\partial}{\partial t}\int_v (w_E + w_H)dv + \int_v \rho_\sigma dv,$$

where $w_E=\frac{1}{2}\varepsilon E^2$ and $w_H=\frac{1}{2}\mu H^2$ are the electric and magnetic energy densities; $\rho_\sigma=\sigma E^2$ is the ohmic power density.

The electromagnetic actuators guarantee high force (torque) and energy densities. In the volume v, the expressions for the field and stored energies are

$$W_F = v\oint_B HdB \text{ and } W_c = v\oint_H BdH .$$

The energy density is given as the area enclosed by the B-H curve, and the magnetic volume energy density is $w_m=\frac{1}{2}\mathbf{B}\cdot\mathbf{H}$ [J/m^3].

MEMS technology has being applied to design high-performance actuators with matching sensors and ICs.

These MEMS systems must ensure *minimal complexity*, implying the use of enabling sensing, actuation and circuitry solutions. The aforementioned approach simplifies the overall system complexity, ensures practicality, enables affordability and safety, etc. As illustrated in Figure 1, the dimensionalities of electromagnetic actuators are less than operational amplifiers and controllers/drivers. The ASICs should be designed to reduce the hardware complexity minimizing the number of the measured variables and feedback used. Control and sensing solutions defines the overall system performance, capabilities, organization, complexity, practicality, affordability, etc. Analog or digital measurements may define design, optimization, implementation and electronics schemes and solutions. Electromagnetic and electrostatic actuators are analog, and, *minimal complexity* MEMS may use analog solutions [1].

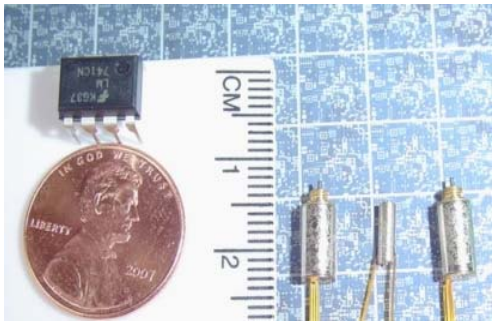

Figure 1. Minimotors with ASICs (controllers/drivers): Actuators are fabricated utilizing MEMS and surface micromachining technologies reducing the actuator size below operational amplifiers

We examine the design and implementation of high-performance drives and servos with state-of-the-art hardware and software. High-torque-density permanent-magnet axial-topology actuators with high-switching-frequency ICs controlled by analog (or digital) controllers are found to be a very promising solution. High performance is achieved by designing *soft switching* PWM converters with two- and four-quadrant power stages.

The control laws are designed to satisfy the specifications imposed, e.g., enhanced stability margins, minimal settling time, high acceleration, accuracy, disturbance attenuation and robustness to parameter variations. The servosystem is depicted in Figure 2.a. The reference signal is the angular displacement. Using the reference θ_{ref} and actual θ_r angular displacements (measured by the high-accuracy sensor), the controller develops PWM signals to drive high-frequency FETs. The output voltage u_a is controlled by changing the duty cycle. Axial topology permanent-magnet miniactuator is documented in Figure 2.b, and a 2×2 cm miniscale hard drive with the proposed actuators is studied [1, 2].

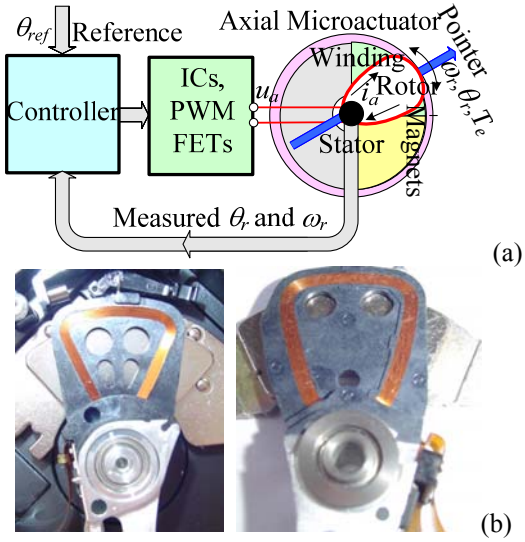

Figure 2. (a) Closed-loop servo: Controller – ICs/Electronics – actuator/sensors – pointer; (b) Images of a miniscale axial-topology hard-drive rotor with planar deposited coils

3. PERMANENT-MAGNET SERVOMOTOR

To rotate the hard drive disk and displace the pointer, we use axial topology direct-drive synchronous actuators with the segmented array of the permanent-magnet strips, see Figures 2. These high-torque-density permanent-magnet actuators exceed performance characteristics achieved by other servomotors [1].

We performed fundamental, analytical, numerical and experimental studies. Graphical user interface (GUI) is developed for actuators in MATLAB. Nonlinearities, disturbances, uncertainties and other factors are examined performing design and optimization tasks. Different control algorithms are studied [1-3]. Comparison of various analog and discrete actuators and servosystem are studied and verified. The results are compared to analysis reported in [1-6].

Analysis is performed using the electromagnetic-mechanical dynamics

$$u_a = r_s i_a + L_a \frac{di_a}{dt} + \frac{d}{dt}\int_s \mathbf{B}\cdot d\mathbf{s},$$

$$J\frac{d^2\theta_r}{dt^2} = J\sum_i T = J\left(T_e - T_{fr} - T_\zeta - \Delta T\right),$$

where u_a and i_a are the armature voltage and current; r_a and L_a are the armature resistance and inductance; J is the moment of inertia; θ_r and ω_r are the angular displacement and velocity; T_e is the electromagnetic torque, $T_e=R_\perp F_e$, $F_e=-Ni_a\int_l B(\theta_r)dl$; N is the number of turns; T_{fr}, T_ξ and ΔT are the friction, stochastic and secondary-effect torques, $T_{fr}=B_m\omega_r$.

The magnetization of permanent magnets defines the expressions for the *motional emf* and electromagnetic torque. The magnets can be magnetized to ensure

$B(\theta_r)=B_{max}\sin^{2q-1}(a\theta_r)$, $B(\theta_r)=B_{max}\tanh^{2q-1}(a\theta_r)$,

or $B(\theta_r)=B_{\max}\text{sgn}[\sin(a\theta_r)]$,
where $B_{\max}$ is the magnetic flux density from the permanent magnets as viewed at the coils; a and q are the technology-dependent integer.

For example, using the practical magnetization, one obtains

$$\frac{di_a}{dt}=\frac{1}{L_a}\left[-r_a i_a-\frac{\left(r_{out}^2-r_{in}^2\right)}{2}NB_{\max}\left(\tanh a(\theta_{L0}-\theta_r)+\tanh a(\theta_{R0}+\theta_r)\right)\omega_r+u_a\right]$$

$$\frac{d\omega_r}{dt}=\frac{1}{J}\left\{l_{eq}NB_{\max}\left[\tanh a(\theta_{L0}-\theta_r)+\tanh a(\theta_{R0}+\theta_r)\right]i_a-B_m\omega_r-T_\xi-\Delta T\right\}$$

$$\frac{d\theta_r}{dt}=\omega_r,\ -\theta_{r\max}\le\theta_r\le\theta_{r\max}, \qquad (1)$$

where $\theta_{L0}=\theta_{r\max}$, $\theta_{R0}=\theta_{r\max}$.

4. Simulation of Closed-Loop Servos

The design, analysis and simulations tasks are performed. The actuator parameters are: N=100, r_a=35 ohm, L_a=4.1 mH, $B_{\max}$=0.5 T, $B_m=2\times10^{-5}$ N-m-sec/rad and $J=1.5\times10^{-9}$ kg-m^2.

The close-loop system performance can be assessed and evaluated using the functional.

$$J_P=\int[q_1|e|+q_2t|e|+q_3|u_a\|i_a|+q_4u_a^2]dt\,,$$

where q_i are the weighting coefficients.

The fuzzy logic controller design uses two inputs (position error signal PES and derivative of PES), and, one output (applied voltage). The membership function for the inputs and outputs are shown in Figure 3. The rule base for the fuzzy inference system is provided in Table 1.

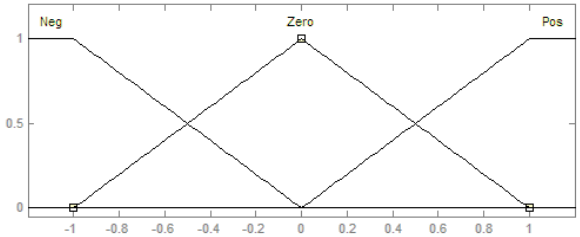

Figure 3. Membership function for inputs and output of a fuzzy control law

Table 1. Fuzzy rules

e / de/dt	Positive	Zero	Negative
Positive	Positive	Positive	Zero
Zero	Positive	Zero	Negative
Negative	Zero	Negative	Negative

For a proportional control law, the proportional feedback gain is k_P=100. For a fuzzy control law, the gain values are derived to be k_u=25, k_e=5 and k_r=0.00001.

The closed-loop system response for square reference θ_{ref}=0.1 rad with frequency 100 Hz is shown in Figure 4. The limits on the angular displacement is $-0.175\le\theta_r\le0.175$ rad. The evolutions of $\theta_r(t)$ and performance functional J_P are shown in Figure 4. Here, q_1=20000, q_2=2000000, q_3=100 and q_4=3 are weighting coefficients. The proportional control law ensures *near optimal* performance.

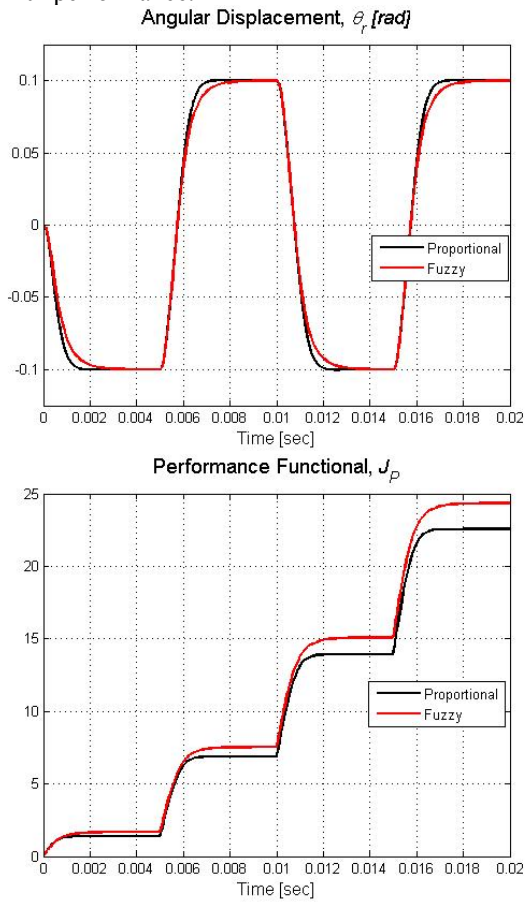

Figure 4. Angular displacement and performance functional

5. Control of Nonlinear Servosystems: Experimental Results

We study a positioning system for a miniscale hard drive. The requirements are: guarantee accurate fast tracking and repositioning; eliminate steady-state positional error (tracking error); attenuate disturbances; minimize the settling time; ensure robustness to parameter variations. The specific feature is the random disturbances due to the perturbations of T_ξ. The SmCo permanent magnets are used as the arrayed magnetic strips. Figure 5 illustrates the mechanical configuration and hardware test bed.

Figure 5. High-performance servo with axial topology servo, sensors, ICs and a controller

The magnitude of the applied voltage u_M is bounded. The FETs duty cycle d_D is bounded as $-1 \le d_D \le 1$. Thus, we have $u_{\min} \le u \le u_{\max}$. As the control variable, we use is the duty ratio of the FETs. Two-quadrant power stage with FETs is used to vary the applied voltage supplied to the phase winding. The angular displacement θ_r is measured by the high-accuracy sensor. The control algorithm is implemented by using analog controllers and microcontroller (clock rate is 20 MHz). The actuator parameters are found to be: N=108, r_a=6.4 ohm, $L_a=3.32\times10^{-5}$ H, $B_{\max}$=0.4 T, a=100, $B_m=5\times10^{-8}$ N-m-sec/rad and $J=1.4\times10^{-6}$ kg-m^2 (the equivalent moment of inertia that integrates the pointer inertia).

Using the tracking error

$e(t)=\theta_{\text{reference}}-\theta_r$, $-\theta_{r\max} \le \theta_r \le \theta_{r\max}$,

analog and digital proportional-integral (PI), nonlinear PI, sliding mode, fuzzy-logic and other control law are designed, examined and tested. For example, the linear and nonlinear PI control laws are

$$u=\text{sat}_{u_{\min}}^{u_{\max}}\left(k_p e(t)+k_i\int e(\tau)d\tau\right),$$

$$u=\text{sat}_{u_{\min}}^{u_{\max}}\left(k_p e(t)+k_{p1}e^{1/5}(t)+k_i\int e(\tau)d\tau+k_{i1}\int e e^{1/5}(\tau)d\tau\right),$$

while the soft-switching sliding mode control algorithm is

$$u=u_{\max}\tanh\left(k_{p2}e(t)+k_{p3}e^{1/5}(t)\right).$$

The design of the nonlinear and sliding mode control laws is performed using methods reported in [1, 2]. In particular, using the positive-definite quadratic Lyapunov function $V(e,x)\ge0$ and solving the inequality

$dV(e,x)/dt \le -q_e\|e\|^2$,

the feedback coefficients are found.

For example, the feedback gains k_{pj} and k_{ij} are found. In general, for $V(e,x)\ge0$, the inequality

$dV(e,x)/dt \le -q_e\|e\|^2$

guarantees the sufficient conditions for stability [1, 2].

The tracking control laws with state feedbacks and sliding mode control algorithms are designed [1, 2]. The dynamics is shown in Figure 6. For

$$u=\text{sat}_{u_{\min}}^{u_{\max}}\left(k_p e(t)+k_i\int e(\tau)d\tau-K\left[i_a \quad \omega_r \quad \theta_r\right]^T\right)$$

with k_p=31 and k_i=24, K=[0.174 2.9 3.4], the settling time is 0.027 sec, and the overshoot is 27%.

The *soft switching* sliding mode control ensures precise tracking with zero steady-state error, while the overshoot is 1%. Figure 6 illustrated the transient dynamics for $\theta_r(t)$ for closed-loop systems with PI control (k_p=20 and k_i=19) and sliding mode control. We tested a miniservo with and without return spring and magnets which are commonly used to ensure mechanical damping. Thus, the most challenging problem is considered. Pointer acceleration and deceleration are achieved by properly controlling the servoactuator which operates at very high efficiency and develops high electromagnetic torque. We conclude that optimal performance and enabled capabilities are achieved.

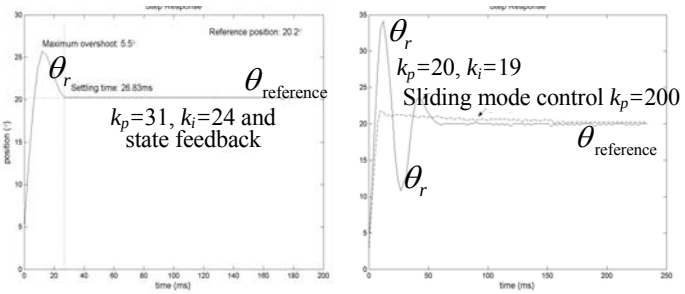

Figure 6. Transient dynamics of the closed-loop servo with the bounded proportional-integral controller laws and *soft-switching* sliding mode control law

6. CONCLUSIONS

High-performance MEMS, which integrate electromagnetic servomotors, sensors and ICs were studied. The major goal of this paper was to solve various design, optimization and implementation problems to design *minimal complexity* system. A fully integrated minidrives and servo (pointing system – sensors – servomotor – ICs – controller) were built, tested and characterized. We reported a systematic procedure in the design of MEMS.

REFERENCES

1. S. E. Lyshevski, *Electromechanical Systems and Devices*, CRC Press, Boca Raton, FL, 2008.
2. S. E. Lyshevski, *MEMS and NEMS: Systems, Devices, and Structures*, CRC Press, Boca Raton, FL, 2002.
3. R. Oboe, A. Beghi, P. Capretta and F.C. Soldavini, "A simulation and Control Design Environment for Single-Stage and Dual-Stage Hard Disk Drives," *IEEE/ASME Trans. On Mechatronics*, vol. 7, no. 2, pp. 161-170, June 2002.
4. H. Numasato and M. Tomizuka, "Settling Control and Performance of Dual-Actuator System for Hard Disk Drives," *Proc. American Control Conference*, June 2001.
5. M. Kobayashi, S. Nakagawa, T. Atsumi and T. Yamaguchi, "High-Bandwidth Servo Control Designs for Magnetic Disk Drives," *Proc. IEEE/ASME International Conf. on Advanced Intelligent Mechatronics*, pp. 1124-1129, July 2001.
6. H. Lin, Q. Li, Z. He and S. Chen, "Development of a Single Coil Coupled Force VCM Actuator for High TPI Magnetic Recording," *IEEE Trans. On Magnetics*, vol. 37, no. 2, pp. 850-854, Mar. 2001.